A Comprehensive Study on Parametric Optimization of Plasma-Sprayed Cr_2C_3 Coatings on Al6061 Alloy

G. S. Pradeep Kumar[1] · **R. Keshavamurthy**[2] · **M. Siva Santosh**[1] · **Siddavatam Narayana Reddy**[1] · **Vijay Tambrallimath**[3]

Abstract Plasma spray, a widely employed thermal spray method, is known for enhancing coatings with heightened microhardness, density, and bonding strength. In this study, Taguchi's approach was applied to optimize processing parameters for plasma spray-coated surfaces, aiming to reduce porosity, increase hardness, and fortify the connection between Cr_2C_3 coatings. The design of experiments method facilitated the optimization of process parameters, utilizing signal-to-noise ratios and ANOVA analysis to assess the significance of each processing parameter and identify optimal parameter combinations. Powdered feed rate and stand-off distance emerged as the two most critical processing variables influencing permeability and hardness, contingent on signal-to-noise ratios. S/N ratio analysis was employed to determine the optimal processing parameters for permeability, hardness, and bonding strength. For porosity, the optimal stand-off distance, powdered feed rate, and current density were identified as 60 rpm, 50 g/min, and 460 amps mm/s, respectively. Exemplary process conditions for hardness included a powdered feed rate of 60 g/min, a stand-off distance of 80 rpm, and a current density of 480 amps. Lastly, for strength properties, the ideal process variables were a stand-off distance of 80 rpm, a current density of 480 amps, and a powdered feed rate of 60 g/min. Despite small differences between projected R2 and modified R2 values in statistical data on permeability, hardness, and bonding strength, the proximity to the one emphasizing the fit of the linear regression used for analysis was evident. Fracture results from the binding strength test postulate mixed adhesion-cohesion type failures in the Cr_2C_3 coatings.

Introduction

Thermal spray surface coatings have grown in popularity as a way to protect structural components and parts from deterioration processes, such as wearing, eroding, scouring, and rusting. The primary goal of developing surface coatings should be to solve the significant financial loss and shortened expected lifespan caused by environmental pollutants in structural applications or constructions. Thermal spray technologies are expected to grow dramatically and be worth USD 17.6 billion by 2027. Currently, the coating is used in a variety of fields, including dentistry, biomedicine, construction, power, and athletics, as well as protective coatings for gas turbines. A desirable coating composed of pure metallic materials, fused self-fluxing alloy, cermet, carbides, and oxides is deposited using appropriate spraying methodology based on the purpose [1–7].

Among all current spraying methods, the plasma spray technique is unique. Plasma surface coatings are reported to have lower permeability than plasma spray coatings and similar chemistry to spray powders [8–10]. The plasma process

✉ G. S. Pradeep Kumar
Pradeepkumar.gs@christuniversity.in

✉ R. Keshavamurthy
Keshavamurthy.r@gmail.com

1 Department of Automobile Engineering, CHRIST University, Bengaluru 560074, India

2 Department of Mechanical Engineering, Dayananda Sagar College of Engineering, Bengaluru 560078, India

3 Department of Automobile Engineering, Dayananda Sagar College of Engineering, Bengaluru 560078, India

also provides increased density, strong bonds, higher surface finishes, increased durability, and increased micro-hardness.

Plasma spraying is a type of thermal spray coating that uses a high-temperature plasma jet to melt and drive particles onto a substrate, creating a dense and firmly attached covering. This method is renowned for its versatility in depositing a variety of materials such as metals, ceramics, and polymers onto different substrate shapes. Plasma spraying offers advantages including fast deposition rate, high bond strength, and the capability to apply coatings at low temperatures to reduce thermal deformation of the substrate [11, 12].

Plasma is used to coat high entropy alloys, tungsten carbides, chromium carbides, Ni-based, and iron-based coatings [13–17]. For example, Reddy et al. [14] reported the production of Ni_3Ti and $Ni_3Ti + (Cr_2C_3 + 20NiCr)$ coatings using the plasma process. The porosity percentages of both coatings were found to be between one and two percent. In a separate study, Shivalingaiah et al. [18] investigated the permeability of Inconel-718 reinforcing with CBN (cubic boron nitride) composite coating. The permeability percentage spectrum for coating reinforcing with CBN from 5 to 20% was determined to be 22–40%. This study revealed that dense surface coatings can be produced using a plasma process with a permeability percent of less than 2%.

Furthermore, in the plasma process, powder particles have a higher kinetic energy, resulting in coatings with low permeability and high binding strengths. Furthermore, higher velocities result in significantly less oxidization of the powder particles, resulting in a compact coating with little to no oxides. On the other hand, Bolelli et al. [19] used high-velocity oxy-fuel and APS to assess the permeability and morphology of Cr_2C_3 coating spray. Fracture propagation across intrusion borders was demonstrated to be simple in APS-sprayed Cr_2C_3 coatings, whereas in plasma sprayed, the splats appear to be firmly bonded to each other. APS had a higher permeability percentage of 6.60% than high-velocity oxy-fuel coatings, which had a permeability percentage of 5.50%. High temperatures, corrosive environments, and repeated slides are all likely to deteriorate parts and cause the comprehensive design framework to fail catastrophically. In these cases, the oxide-based coating is frequently chosen to achieve the intended life span and improve efficiency. Singh et al. [20] pin-on-disk studies revealed that Cr_2C_3 coatings had lower accumulated wear than $Al_2O_3 + TiO_2$ composite coatings, according to ASTM G99-90. It was explained by the dense fluid layer formed when splats were plastically deformed, which resulted in lower wear loss than $Al_2O_3 + TiO_2$ composite coatings. The oxide with the best microhardness, lowest COF, lowest corrosion rate, and lowest wear rate is chromium oxide (Cr_2C_3) [21, 22]. Fernandez et al. [23] investigated friction and tribology of AISI-D2 countering surfaces and Cr2C3 coatings using a block on ring tribometer. Cr_2C_3 coatings outperformed steels in terms of wear rates at various sliding velocities and loading conditions. Zamani et al. [24] measured the hardness and binding strengths of Cr_2C_3, Al_2O_3-3%TiO_2, and Cr_2C_3/Al_2O_3/3%TiO_2 coatings. In comparison to the other coating materials, Cr_2C_3 coatings had the highest hardness and binding strength, measuring 1380HV and 51 MPa, respectively. Conz.e et al. [25] compared the hardness and wear rates of several coating materials, including TiO_2, Cr_2C_3, Al_2O_3/TiO_2, and Al_2O_3/Cr_2C_3. The Cr_2C_3 coating had the highest mechanical strength and the lowest wear rate of any coating, measuring 1250HV.

The article by Reddy et al. [26] describes how Ni_3Ti and $Ni_3Ti + (Cr_2C_3 + 20NiCr)$ coatings were created using the plasma technique on titanium alloys ASTM-B265 (Ti-15) and AISI-420 stainless steels (MDN-420). They investigated coating materials' morphology, microhardness, and high thermal oxidizing properties. The coating's morphology was thick, with layers that resembled lamellar structures. Because of the higher concentration and bonding strength among specific splats of protective coatings, the coating had a much higher micro-hardness than the substrates. The oxide scales in Ni_3Ti and $Ni_3Ti + (Cr_3C_2 + 20NiCr)$ coating materials were made up of a variety of oxides, including the phases NiO, $NiCr_2O_4$, and Cr_2C_3, according to research on the cyclical oxidizing of Ni_3Ti and $Ni_3Ti + (Cr_2C_3 + 20NiCr)$ coating materials. In the case of Ni3Ti coating materials, a compacted and protective NiO phase forms; in the case of $Ni_3Ti + (Cr_3C_2 + 20NiCr)$ coating materials, the excess weight NiO and Cr_2C_3 phases remain stable and demonstrate a moderate oxidation process at extremely high temperatures.

Goyal et al. [27] investigated the erosion-corrosion performance of plasma spray coating on CA6NM hydroelectric turbine steels under different concentrations of various variables. To achieve homogeneous layer coatings, composite powders containing Cr_2C_3-50%Al_2O_3 were coated on CA6NM steel specimens. The surface finish, permeability, and micro-hardness of the specimens were examined without the coating. The surface morphology of the coating material was evaluated, and the uncoated specimens were examined using a scanning electron microscope and elemental dispersive spectroscopy. Eroding experiments were carried out in hydro-accelerated conditions on a self-made eroding experimental setup. The investigation revealed that the major factors influencing the rate of erosion of these coatings were their velocities, impact angles, and slurry content. The particle size had the least effect on the erosion rate. High-velocity oxy-fuel-coated CA6NM specimens demonstrated greater corrosion resistance than plasma-coated specimens due to their increased microhardness.

Reddy et al. [28] used the high-velocity oxy-fuel process to apply Ni_3Ti and $Ni_3Ti + (Cr_2C_3 + 20NiCr)$ coating to gas

turbine-dependent ASTM B-265 titanium (Ti1$_5$) and AISI-420 stainless steels (MDN-420) substrate material. Thermocyclic elevated temperature corrosion tests were carried out at 923 K for approximately fifty cycles in a molten salt environment of Na2SO4 40% V2O5. The thermogravimetric measurements were used to investigate the high-temperature corrosion dynamics of uncoated and coated Ti substrates as well as stainless-steel substrates. In terms of gaining weight per unit surface area, coated substrate material outperformed uncoated substrate material in heat corrosion resistance. The surface topography of substrate material that was both uncoated and coated was examined using SEM and elemental dispersive spectroscopy. The formation of various oxides and compounds was investigated using X-ray diffraction. Uncoated sample surfaces had some micro-spalling, whereas coated substrate surfaces had a layer of protecting oxides. When ternary NiCr2O4 protecting oxides are present on the Ni$_3$Ti + (Cr$_2$C$_3$ + 20NiCr) coated substrate, the penetration of corrosion products inside the coating is reduced.

Goyal et al. [29] investigated the high-temperature corrosion nature of Cr$_2$C$_3$ composite coatings reinforcing with carbon nanotubes (CNTs) in the boiler atmosphere of a power generation plant under cyclical thermally load circumstances at 1173 K. The plasma technique was used to apply the coating, with the carbon nanotube concentration ranging from one to eight weight percentage. The impact of varying carbon nanotube content (from one to eight weight percentage) on the response of high-temperature corrosion was compared using weight variation assessment, and the corrosion products were examined using XRD, SEM, energy dispersive spectroscopy, and cross-sectional research methodology. The results demonstrated that in a real boiler environment characterized by high temperatures, a change in the initial concentration of carbon nanotubes improved the corrosion protection of surface coatings. The coatings developed protective oxide scales and experienced less weight increase throughout the trial. The concentration of carbon nanotubes in the coating matrix decreased corrosion protection when exposed to high-temperature corrosion.

Cho et al. [30] used a cobalt-based plasma thermal spray to coat Inconel718 (IN718) powders with Tribaloy-800 (T-800). The ideal coating procedure (OCP) was discovered by analyzing the surface characteristics of 16 coatings generated by the Taguchi software. Spray operations had a significant impact on both surface microhardness and permeability, which ranged from 560 to 630 HV and 1 to 2.7 percent, respectively. At a 5-inch spraying range, the oxygen flow rate of microhardness was found to be 38 FMR, the hydrogen flow rate was 75 FMR, and the feed rate was 30 g/min. The addition of the Nickel–Chromium binding layer significantly increased the T-800 coating's temperature resistance while also slightly increasing its bonding strength to the substrates. The frictional and tribological behaviors were investigated using a reciprocal sliding examination at 298 K and enhanced temperatures of 811 K. The coefficient of friction and wear indications of the coating were lower than those of the IN-718 substrates at both 298 K and 811 K. The lubricating effect of cobalt oxides generated on the sliding surfaces reduced the friction coefficients and wear traces of IN-718 and coatings as surface temperatures rose. T-800 coatings were therefore strongly recommended as a longevity enhancement coating to protect sliding surfaces, such as high-speed spindles.

Thermal spray of fine feedstock powder particles enables the deposit of cermet coating materials with significantly improved properties in both research and industry. The lower weight and higher surface-to-volume ratio of tiny particulates, on the other hand, make them difficult to jet and exhibit poor flow properties during feeding. The use of new thermal spraying apparatus, as well as an appropriate examination and optimization of the processing parameters, is critical for effectively processing finer particles while maintaining the crystal structures of the feedstock materials in the finished coating morphologies. Tillman et al. [29] used tiny 75% Cr$_2$C$_3$-25%(Ni$_{20}$Cr) powders (8 + 2 m) in plasma spray tests to create finely patterned, wear-resistant cermet coating materials. In order to model the deposition effectiveness of the procedure and the most important coating characteristics, Plackett-Burmans, Fractional-Factorials, and Central Composite designs have been used in the mathematical design of experiments. Recognizing one of the most critical processing parameters with linear, quadratic, and interaction effects is essential. Those responder parameters were combined using the concept of performance criteria and desired indices in an attempt to identify processing parameter pairings that produce either the best overall performance or, at the very least, the best balance. Validation studies in the determined optimum produced results that were quite satisfactory, if not excellent. The coating materials had 1.7 percent porosity, Ra = 1.9 m surface roughness, and a mean hardness of 1004HV. A higher deposition effectiveness of 71% was also possible.

Several studies show that standalone Cr$_2$C$_3$ coatings have better properties than composites or other individual ceramic counterparts. Furthermore, Cr$_2$C$_3$ and its composite coating materials are well known for their superior resistance to oxidation, corrosion, and galvanic corrosion at high temperatures [26–31]. They provide strong protection to the substrate against the majority of corrosive conditions and are insoluble in acid, alcohol, and alkalis.

This study utilizes Taguchi's approach to optimize Cr$_2$C$_3$ coating processes by plasma spraying. The main focus is on decreasing porosity while improving hardness and bonding strength. The study provides novel perspectives on processing factors, determines the best parameter combinations, statistically verifies outcomes, and examines failure

processes, offering a thorough structure for enhancing coating performance.

Experimentation

Powders and Spraying

To deposit the substrate, Cr_2C_3 powders with diameters ranging from 5 to 30 microns were used as feedstock powders. Scanning electron microscope (SEM) photographs, elemental dispersive spectroscopy (EDAX) compositional analysis maps, and X-ray diffraction (XRD) maps of the obtained Cr_2C_3 powders are shown in Fig. 1a-c. The EDAX maps revealed that the major constituents of Cr_2C_3 powder particles were oxygen and chromium, with no other constituents detected, indicating high purification. In the micrographs, the visible powdered granules had an angular and uneven microstructure. The substrate for Cr_2C_3 coatings was hot-rolled AA6061 aluminum plates that had previously been grit-blasted with alumina grits. The Cr_2C_3 was coated using Sulzer-Metco 3 MB Plasma torch at M/s Spraymet Technology Private Limited, Bangalore. The thickness of 200 microns was deposited on the substrate. The main gas argon was used at a flow rate of 25 L/min, and the torch power was set at 20 kW based on the current and voltage parameters.

Design of Experiments

As previously stated, the Taguchi L9 orthogonal matrix was used to investigate the effects of three primary variables: stand-off distance, gunpowder feed rate, and current density. Table 1 shows how the investigations are set up with three factors and three classes. Furthermore, the tests were performed using the Taguchi L9 orthogonal array, as shown in Table 2. S/N, or signal-to-noise ratio (S/N), was calculated using testing data generated by the Taguchi technique. Permeability percentage is one of the primary factors evaluated in the coating. To have strong mechanical properties such as higher microhardness and bond strength, the coating must have a low permeability percentage. The maxim "smaller the better" has been considered for such a S/N ratio requirement. According to references [30, 31], the permeability and microhardness of coatings, for example, have an inverse relationship. In order to have the greatest amount of microhardness, the coatings must have less permeability. According to the source [32], as porosity decreases, so does the corrosion rate of coatings. To protect the substrate material from corrosive environments, impervious coatings must be applied. Because it is essential to have admirable traits, the S/N ratio requirement of "bigger the greater" was taken into account for the second and subsequent situations, hardness,

and bonding strength. As previously described, a statistics program called MINITAB-13 was used to determine the impact of each variable on these attributes. The testing data were run through an analysis of variance (ANOVA) using the same program to identify each parameter's important variable and percent contribution. The parameter has a greater impact on coating characteristics as the percentages increase. Every parameter's percentage contribution that is less than 5% is ignored because it is meaningless. Every parameter pairing in Taguchi's L9 orthogonal matrix was tested three times in total.

Characterization of Coatings

Following a bond strength experiment, a SEM (Makers: Tescan-Vega3) was used to examine the microstructure, cross-section characterization, and coating surfaces of Cr_2C_3 powdered particles. Several processing factors were investigated, including permeability in the applied coating, microhardness, and bonding strength. The permeability percentages of the produced coatings were determined using the ASTM-E-2109-01 (Mode A) test procedure. The characterization samples were prepared using standard metallographic techniques. To study the compositional analysis of powders, the elemental dispersive spectroscopy (EDAX) feature in SEM was used, and X-ray diffraction was used to determine the intermetallic behavior of Cr_2C_3 powdered particles.

The microhardness tests were carried out on polish-coated specimens using a Vicker's hardness tester in accordance with ASTM-E-92 standards (Model-Metsonic). The specimens were subjected to 0.1 kg loads for 25 s of dwell time; the mean number of indentations is shown below. An experiment on bonding strength was carried out to investigate the binding between Cr_2C_3 coatings and the AA6061 aluminum alloy substrate. This tension adhesion experiment was carried out in accordance with ASTM-C633 standards, with displacement rates of 1 mm/min [12]. The tension adhesion tests were carried out on a computer numerically controlled (CNC) tension testing setup capable of producing 100 kN. To ensure the mean bonding strength between the Cr_2C_3 coatings and the AA6061 aluminum alloy substrate, tension experiments were performed in triplicate. The fractured specimens were then examined using a scanning electron microscope to study the fracture features.
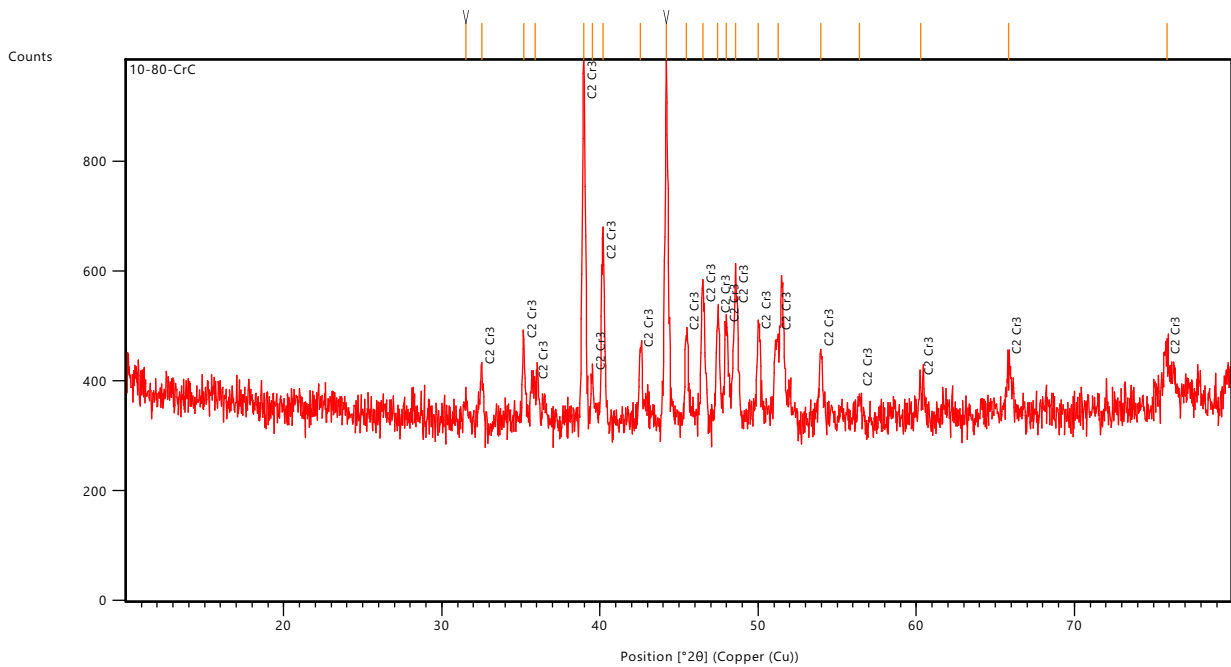
Results and Discussion

The cross-section of the scanning electron microscopic image of the Cr_2C_3 coating on the AA6061 aluminum alloy substrate is shown in Fig. 2. The Cr_2C_3 coating shown in the microstructure was created with the following settings: powder feed rate of 50 g/min, standoff distance of 70 rpm,
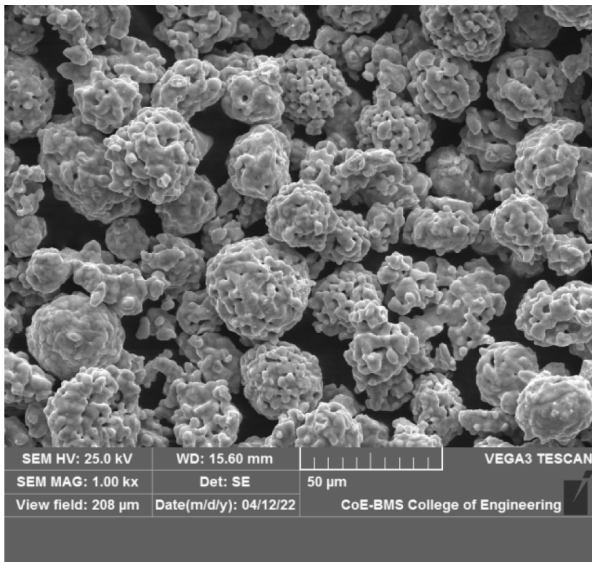
(a)
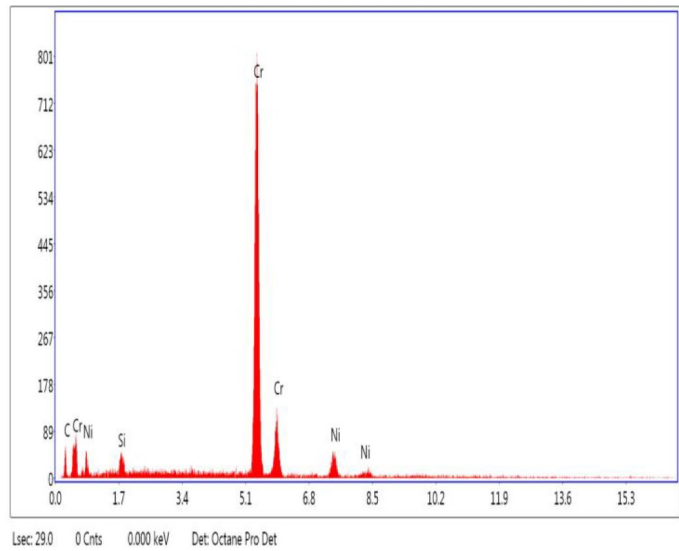
(b)

(c)

Fig. 1 **a** SEM and **b** EDS of as received Cr_2C_3 powder particles **c** XRD of Cr_2C_3 powder particles

and current density of 250 mm/s. The coatings appear to be dense and solid, with good adhesion to the substrates. Lamellar boundaries could be seen when the structure was pushed closer to the AA6061 aluminum alloy substrate. Only a few micro-porosities are visible near the upper layer; no intrusion borders or fissures are visible. Very low

impact velocity and temperatures can often result in barriers between splats, which can have negative consequences such as lower microhardness or weak bonding to the substrates. However, neither the interplay border nor the micro-cracks emanating from these areas can be seen in the Micrographs at this time. After measurements were taken at several

Table 1 Levels of plasma process parameters

Code	Parameter	Level		
		1	2	3
A	Stand-off distance (mm)	60	70	80
B	Powder feed rate (g/min)	50	55	60
C	Current density (Amps)	460	470	480

locations, the average film thickness was discovered to be 200 microns. Table 3 shows the porosity, microhardness, and bonding strength for various configurations of the Taguchi L9 orthogonal matrix characteristics.
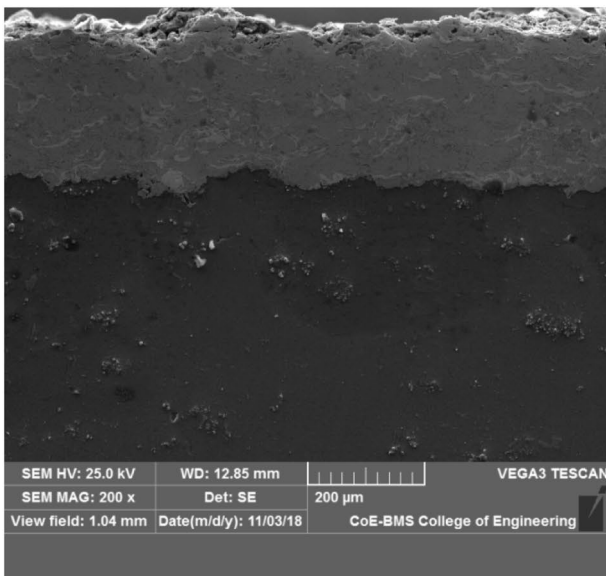
S/N Ratio

The S/N ratio is utilized to determine how far performance requirements have deviated from the target values. Typically, the S/N ratio equation is expressed as [31, 32];

$$\eta = -10 \log \text{(mean square deviation)}$$

Varied performance parameters have a different mean-square variances. Three classifications such as "smaller are better", "bigger is better" and "nominal the better" are used to categorize the performing characteristics. In this instance, it is investigated how significant coating properties like permeability, microhardness, and bonding strength. Reduced permeability in coatings is known to be advantageous and

Table 2 Experimental results for porosity, microhardness and bond strength

Run	Stand-off distance (mm)	Powder feed rate (g/min)	Current density (Amps)	Bond strength (N/mm^2)	Porosity %	Hardness (VHN)
1	60	50	460	25.5	7.2	609.0
2	60	55	470	29.8	3.2	625.0
3	60	60	480	38.9	5.1	599.0
4	70	50	470	32.2	2.8	631.7
5	70	55	480	41	5.8	639.1
6	70	60	460	29.6	5.1	624.9
7	80	50	480	33.9	5.5	633.0
8	80	55	460	31.8	1.4	655.0
9	80	60	470	21	2.9	634.6

(a)
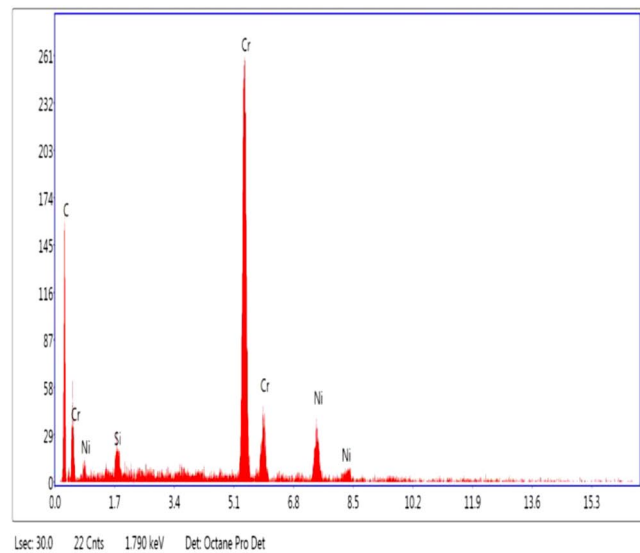
(b)

Fig. 2 **a** SEM and **b** EDAX pattern of cross section of Cr2C3

Table 3 S/N ratio response for porosity

Parameter	Level			Delta	Rank
	1	2	3		
Standoff distance (mm)	−13.80	−13.632	−11.407	4.808	2
Powder feed rate (g/min)	−12.788	−9.431	−9.431	4.201	3
Current density (kg/mm^3)	−8.993	−12.517	−14.742	5.311	1

desired from a mechanical, wear, and corrosive standpoint. With this in perspective, the adage "smaller is better" was much more appropriate. permeability and a similar procedure were used to create a dense covering with a small percentage of porosity. In this approach, the S/N ratio is expressed as,

$$\eta = -10\log\left\{\frac{1}{n}\sum_{i=1}^{n}Y_i^2\right\} \tag{1}$$

In this, the n represents the number of examinations, and 'Yi' is the permeability number for the ith experiment. Additionally, the work's second goal is to achieve excellent micro-hardness and bonding strength levels, and also for this means that the productivity attribute described above would be false. In this aspect, the adage "bigger is better" is applied to both strength properties and micro-hardness. The *S/N* ratio equation for these characteristics is as follows;

$$\eta = -10\log\left\{\frac{1}{n}\sum_{i=1}^{n}\frac{1}{Y_i^2}\right\} \tag{2}$$

The micro-hardness and bonding strength values are represented by the letter "Yi" in this case, and the *S/N* ratio for empirical observations and response Tables is calculated using Eqs. 1 and 2. Tables 3, 4, and 5 show the characteristics of each coating. Each Table displays the delta value and ranking of each process parameter. The delta value represents the difference between the greatest and lowest means of each process parameter. A higher delta value indicates that the process parameter has a significant impact on the coating qualities. The *S/N* ratio responses for permeability

Table 4 S/N ratio response for microhardness

Parameter	Level			Delta	Rank
	1	2	3		
Standoff distance (mm)	55.72	56.01	56.13	0.41	1
Powder feed rate (g/min)	55.91	56.12	55.84	0.28	2
Current density (kg/mm^3)	55.98	55.99	55.90	0.10	3

Table 5 S/N ratio response for bond strength

Parameter	Level			Delta	Rank
	1	2	3		
Standoff distance (mm)	29.80	30.61	29.03	1.58	2
Powder feed rate (g/min)	29.63	30.60	29.22	1.37	3
Current density (kg/mm^3)	29.20	28.70	31.55	2.86	1

in Table 4 show that, while powder feed rate has no effect on coating permeability, current density has a significant effect. This is primarily because the ideal current density ensures complete melt of Cr_2C_3 particles while decreasing permeability percentages. Numerous studies have shown that the current density has a significant effect on particulate temperatures and in-flight speed, which determine permeability and mechanical properties. Qin et al. [33] optimized the high-velocity oxy-fuel technique settings to produce a corrosion-resistant iron coating. The results revealed that the current density or standoff distance had the greatest impact on the permeability of the coatings. The interesting thing to note in this work clearly lends credence to the assertion stated in this study.

Second, similar to the permeability results in Table 4, the results for micro-hardness showed similar S/N ratio responses. The relationship between standoff distance, permeability, and micro-hardness is obvious. Mechanical properties such as micro-hardness are determined by the degree and nature of the coating's permeability and fissures (as shown in Fig. 2). Cr_2C_3 particles were completely melted, resulting in thick coatings with low permeability and no visible fissures. These coatings have increased stiffness, which raises the overall micro-hardness [35]. Table 5 shows that for a strong connection, standoff distance has little influence while current density has a significant influence. In this case, bonding strength and current density are related. Any change in current density during spray can have a negative impact on heat exchange as well as powder impact, resulting in poor splatter development and high permeability levels. The optimal current density ensures that particulates receive an adequate amount of heat energy and that melting is complete. As a result, the porosity of the coatings will be reduced, splatter development will be improved, and bond strength will be increased.

Figure 3a-c shows the primary impact graphs for the S/N ratios for bonding strength, micro-hardness, and permeability (c). Figures show that a standoff distance of 60 rpm, a powdered feed rate of 50 g/min, and a current density of 460 amps are the ideal process variables in Example 3(a). A decrease in droplet temperatures and re-solidification may occur if the standoff distance increases during the spraying operation. Furthermore, the in-flight velocities of melted droplets decrease, resulting in weak splat-to-splat binding.
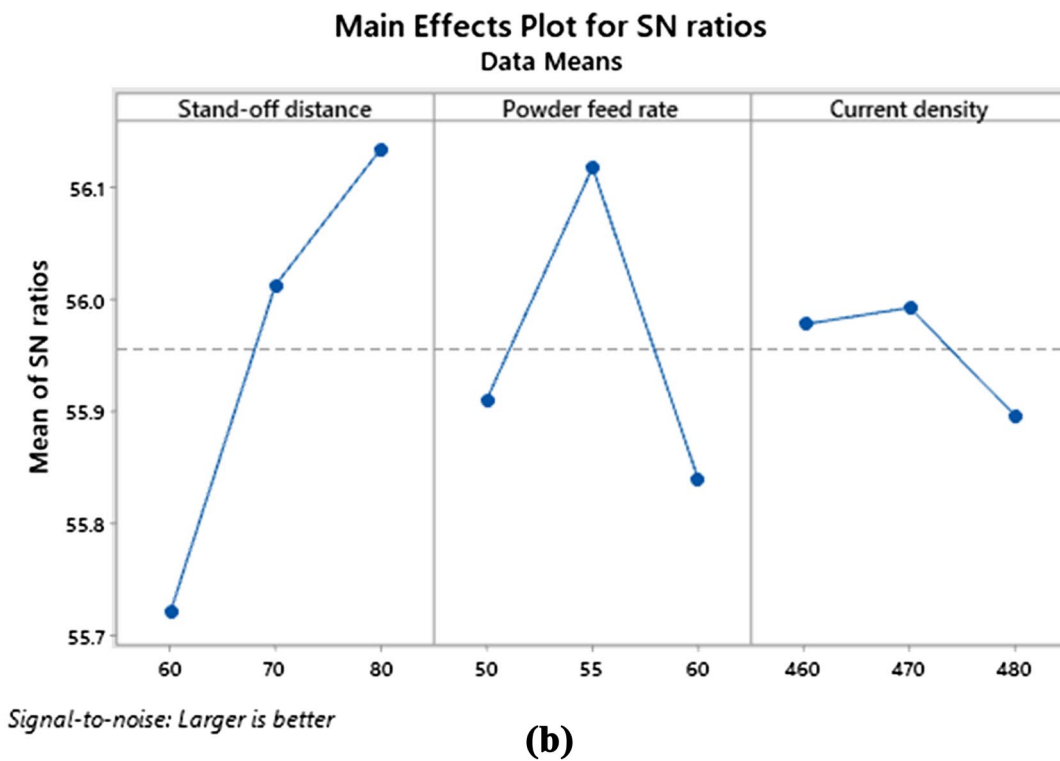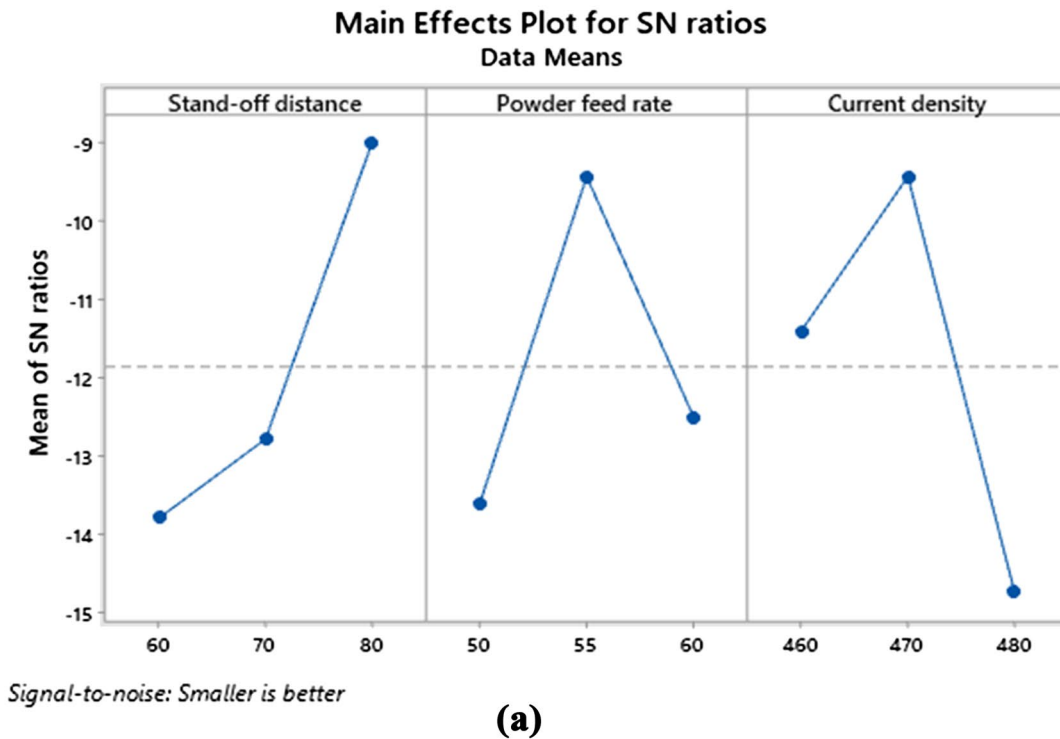
Fig. 3 Main effect plots for S/N ratios for **a** porosity, **b** microhardness and **c** bond strength

The decrease in temperature and impact velocity results in a significant increase in coating permeability. As a result, using reduced standoff data to achieve porosity at a lower level is recommended. To achieve high micro-hardness, the standoff distance should be 300 rpm, the powdered feed rate should be 60 g/min, and the current density should be 470
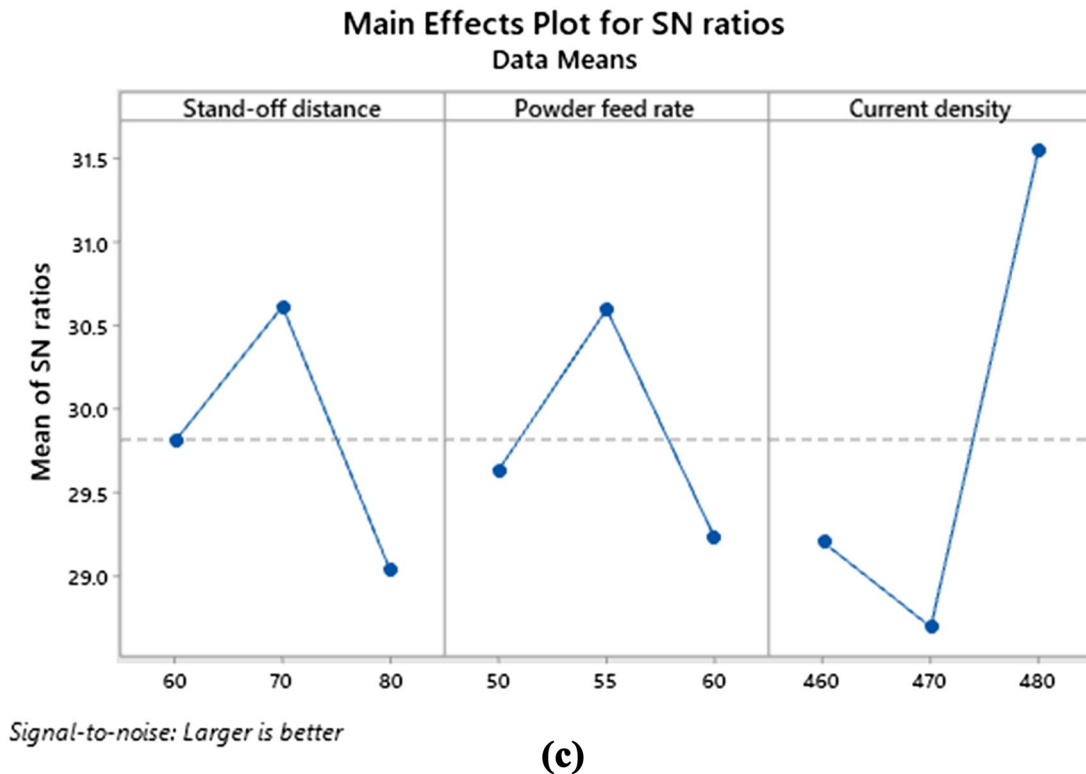
Fig. 3 (continued)

amps (as shown in Fig. 3b). The more powder in the coating, the more compact and denser the coating will be. More passes are required to achieve the desired coating thickness with a reduced powdered feed rate. Because of the high likelihood of tiny particles flying off, porosity develops in the coating, lowering the micro-hardness rating. Last but not least, the ideal processing parameters configuration, as shown in Fig. 3c, includes 80 rpm standoff distance, 60 g/min powder feed rate, and 480 amps current density. As the stand-off distance and powdered feed rate increase, so does the coating's bonding strength. The higher feed rate keeps tiny powder particles from deviating and landing on the substrates. The Cr_2C_3 splats have excellent adhesive strength to the AA6061 aluminum substrate due to their low permeability and thick deposition. The majority of the adhesiveness is commonly attributed to the binding between the Cr_2C_3 coatings and the AA6061 aluminum alloy substrate. Because of the energy delivered by supersonic speed hits, it is possible to achieve high bonding strengths using the high-velocity oxy-fuel approach. The bonding between Cr_2C_3 coatings and AA6061 aluminum alloy substrate will be insufficient and inefficient if imperfections such as porosity and fractures appear at the interfaces, as these are the primary initiation locations of failures. Numerous studies have shown that as permeability increases, the cohesive strength, adhesion, and micro-hardness of applied coatings all decrease dramatically

[37, 38]. If the permeability is low, the coating is more likely to adhere to the substrates.

Furthermore, the shorter length causes flaws, such as porosity, un-melted particulates, and splat borders. This is primarily due to the fact that Cr_2C_3 particulates tend to stay in the flame for shorter periods of time, which may prevent them from melting at the proper temperature or reaching the substrates with enough inflight velocity to form strong bonds [39]. Greater standoff range is recommended as the ideal process feature for strong adhesiveness. The interesting thing to note here is that it is consistent with Praveen et al. [40].'s research on Taguchi technique-based processing parameter optimization. The NiCrSiB/WC-Co coating spray by the high-velocity oxy flame demonstrated higher abrasion resistance when the length was 300 mm. It was explained by the fact that at this stand-off distance, the granules are subjected to extremely high temperatures and velocities, which aid in the depositing of compacted and dense coatings. Figure 4a-c also shows the response maps for interfacial adhesion, micro-hardness, and permeability. To assess the effect of the process variables on the three coating properties, the generated three-dimensional trends were compared to the process variables. The apex represents the greatest impact, while the dip represents the least [41]. While the iterative approach or apex, as shown in the contour plot, results in greater permeability in the formed

Surface plot of Porosity vs SOD, PFR

(a)
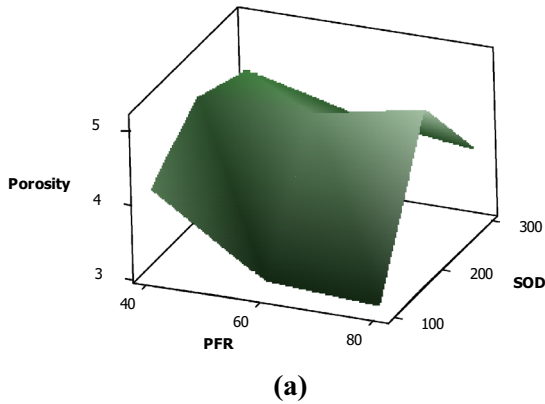
Surface plot of Mocro-hardness vs SOD, PFR

(b)
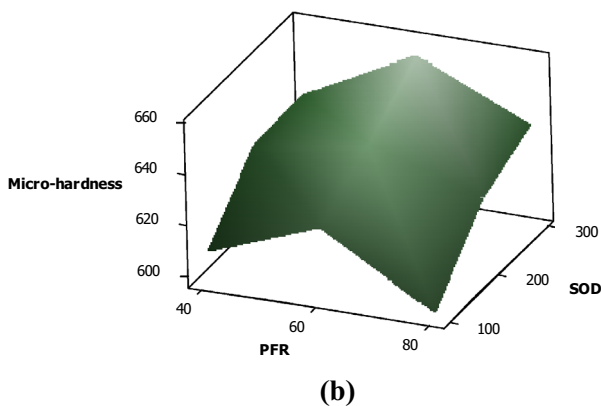
Surface plot of Bond Strength vs SOD, GS
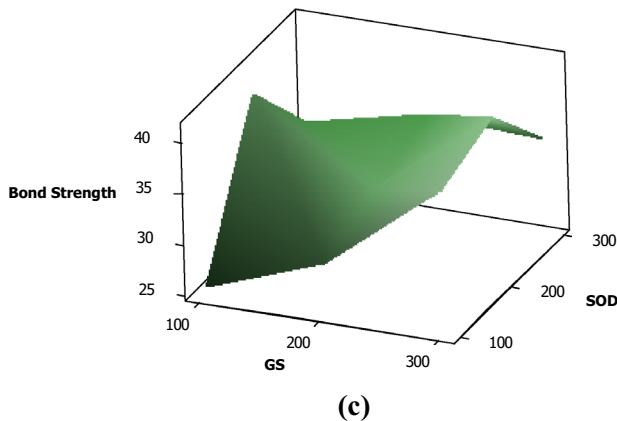

(c)

Fig. 4 Response graphs for **a** porosity, **b** microhardness and **c** bond strength

coatings, the greater and lesser degrees of stand-off distance result in decreased permeability. When it comes to micro-hardness, as shown in Fig. 4b, the contoured graph demonstrated that the peak level increased as the powder feed rate and standoff distance increased. This implies that

increasing both processing parameters causes more Cr_2C_3 powders to strike the surface faster, forming a compact and thick coating that improves coating micro-hardness. As the current density increases, the binding strength eventually reaches its maximum (as shown in Fig. 4c). However, the responsiveness of the graph troughs at a greater stand-off distance, implying a reduction in coating adhesion.

Analysis of Variance (ANOVA)

ANOVA analysis is another critical step in determining the most important processing parameters that significantly affect strength properties, micro-hardness, and porosity. The Fisher's factor (F), which is calculated for each of the processing parameters, is the most important factor in an ANOVA study. This ratio represents the relationship between the mean-square of processing parameters and the mean-square of an error. If the F value is less than 0.05, those characteristics are considered non-significant and are ignored. Tables 6, 7, 8 show the ANOVA results for the permeability, micro-hardness, and strength properties of Cr_2C_3 coating materials. Tables 6 and 7 show the permeability and micro-hardness, respectively, and the F value for stand-off distance is greater than other factors with a significant impact, though powder feed rate appears to have the least. Furthermore, while standoff is the most important factor in bond strength, the impact of distance is the smallest. Table 9 also includes statistical data for strength properties, micro-hardness, and permeability. The R2 value is typically expected to be close, implying that there should be as little variation as possible between the experimental and estimated values [35]. Permeability's corrected R2 value is 98.7%, compared to the projected R2 value of 99.7%. Similarly, the expected R2 and modified R2 values for micro-hardness are 99.96% and 99.85%, respectively. The difference between the two numbers is very small and close to one. In terms of micro-hardness, the porousness of the expected R2 values and the corrected R2 values agree well. However, the expected R2 and corrected R 2 values for strength properties are 82.25% and 29.00%, respectively. According to the corrected R2 value of 99.85%, the regression model was unable to account for 17.7% of the residual variation. Although the variation in bond strength is greater than that in permeability or micro-hardness, it is still close to a corrected R2 value, demonstrating the model's suitability. This demonstrates that the empirical relationships developed are accurate and could be used to predict the permeability and micro-hardness of Cr_2C_3 coatings. The coating micro-hardness can also be predicted using this accuracy of fit for a given value of porosity.

Table 6 ANOVA results for porosity

Source	DF	Seq SS	Adj SS	Adj MS	F	P
S D	2	38.54	38.54	19.27	0.82	0.549
P F R	2	28.41	28.41	14.21	0.61	0.623
C D	2	43.24	43.24	21.62	0.92	0.520
Error	2	46.86	46.86	23.43		
Total	8	157.05				

Table 7 ANOVA results for microhardness

Source	DF	Seq SS	Adj SS	Adj MS	F	P
SD	2	0.272787	0.272787	0.136393	1718.42	0.001
PFR	2	0.126551	0.126551	0.063275	797.20	0.001
C D	2	0.016244	0.016244	0.008122	102.33	0.010
Error	2	0.000159	0.000159	0.000079		
Total	8	0.415740				

Table 8 ANOVA results for bond strength

Source	DF	Seq SS	Adj SS	Adj MS	F	P
SD	2	3.748	3.748	1.874	0.84	0.544
P F R	2	2.984	2.984	1.492	0.67	0.599
C D	2	13.950	13.950	6.975	3.13	0.242
Error	2	4.463	4.463	2.232		
Total	8	25.146				

Table 9 Statistical results for coating characteristics

Response	R-squared	Adjusted R-squared
Porosity	70.16%	0.00%
Microhardness	99.96%	99.85%
Bond strength	82.25%	29.00%

Characterization of Prepared Samples

SEM was used after bond testing to determine the mode of fracture in the fractured areas and how it related to the process variables. Figure 5a-d shows scanning electron micrographs of Cr_2C_3. All coated specimens revealed a mixture of adhesion and cohesion type fractures, which occurs when the adhesive fails first and the coating fractures, based on the microstructures. Figure 6 clearly depicts this type of fracture. As a result, the fracture was caused by cohesive failure accompanied by adhesion failures, particularly at the junction between laminae and partially or slightly melted particulates. The failure in covering 1, as shown in Fig. 5a, combines adhesion and cohesion. There was no evidence of massive failure, and there were few coating fragments left on the surface layer. Coating 6's primary failure mechanism, on the other hand, was identical to coating 1's, with remnants of the coating discovered on the substrate surface (can be seen

in Fig. 5b). The primary difference between coatings 1&6 is that the contact area of coating 6 was significantly larger than that of coating 1. However, when coating 7 is considered, the coating actually covered more of the surface layer (as shown in Fig. 5c). Figure 5d shows that Coating 9 had a much lower percentage of coating residues on the surface layer than the other coating. A small number of patches of the coating were discovered to be distributed throughout the surface layer.

As can be seen, each of the coatings demonstrated mixed-mode failures, which frequently begin with adhesion fracture and are followed by epoxy detachment. The junction seen between laminae, as well as other interactions between laminae and un-melted particulates, are some of the areas where the coating fails, though it begins at the coating and substrate interfaces. If the lamellas do not adhere well to one another or if there are more un-melted particulates in the coating, there are several possibilities for poor interfacial adhesion. As seen in the scanning electron microscopy images, the coating is destroyed in small clusters, indicating that the fractures spread from the coating-substrate contact to the porous junctions of lamella-un-melted particulates. Cohesiveness between laminae and unmelted particles is frequently weak here, and additional strain may result in localized fractures. The scanning electron micrographs of coatings 1 and 6 show only minor coating remnants on the
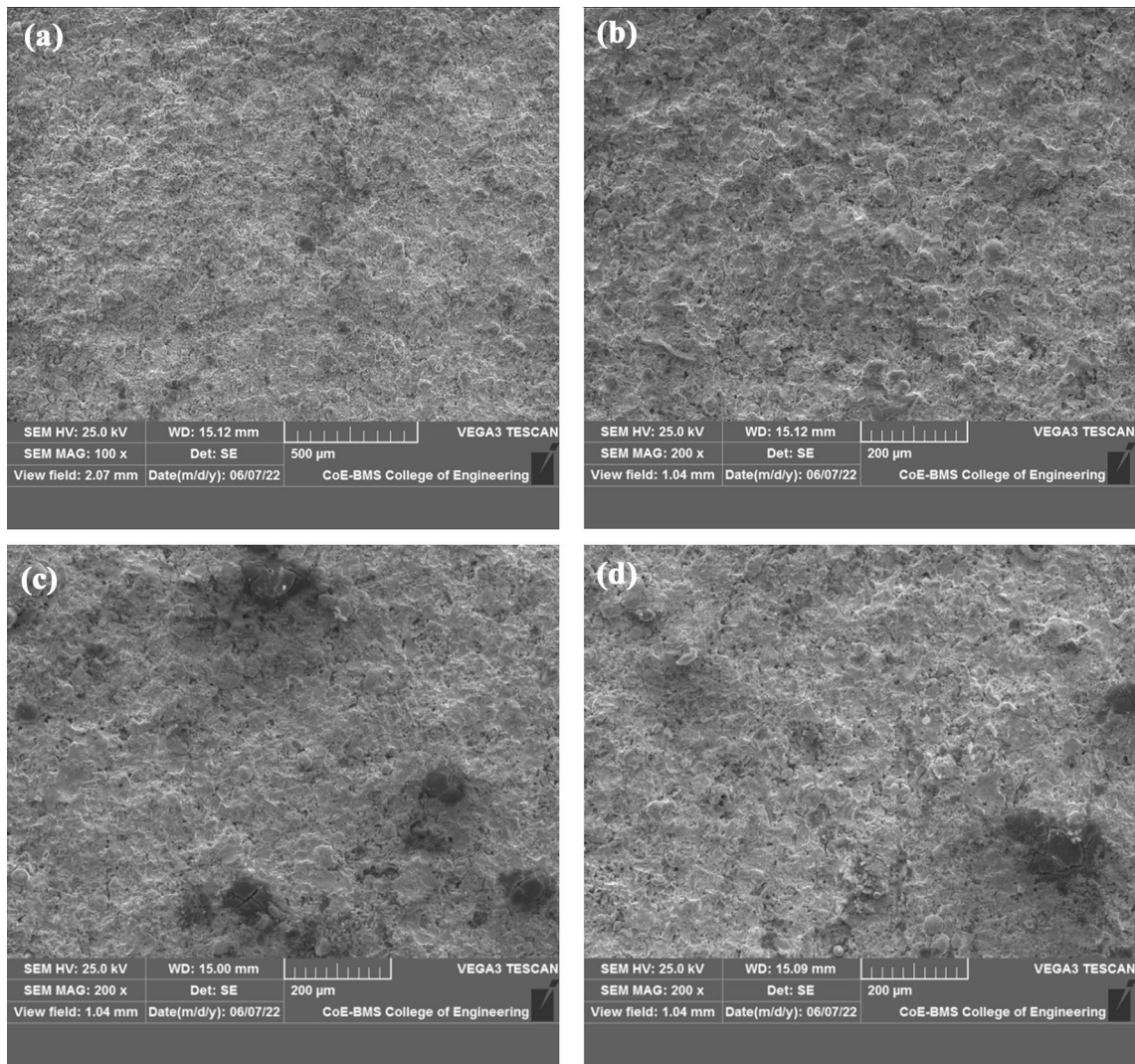
Fig. 5 Fracture surface of Cr_2C_3 coatings at standoff distance (mm), powder feed rate (g/min) and current density (amps) of **a** 60, 50, 460; **b** 70, 60, 480; **c** 80, 50, 460 and **d** 80, 60, 480

substrate, whereas coating 7 has a coating that covers a larger surface area. The bond strength values shown in Table 2 provide additional support for this claim. Bond strengths for coatings 1, 6, 7, and 9 are 25.5 MPa, 29.6 MPa, 33.9 MPa, and 21.0 MPa, respectively. Coating 7 had a higher bond strength value and more coating fragments overall [42]. Photographs of the entire fragmented surface were also obtained to provide a better understanding of how coating fracture began at the coating-substrate interface. Figure 6a and b shows images of coatings 7&9 obtained after the bonding test (b). The highlighted yellow area for the two coatings emphasizes the failing start at the intersection.

Because of metallurgical binding, mechanical clamping, and current density, the Cr_2C_3 coatings and the AA6061 aluminum alloy substrate have a stronger bond [42]. When there is a higher intensity velocity and fully molten Cr_2C_3

particles, the substrate area is more likely to be locally melted. In addition to this preliminary grit blowing, when highly propulsive fragments are catapulted at the substratum, the interaction temperature may rise due to the transformation of that energy into thermal energy upon influence. Molten material may erupt from the particulate (coated) side as well as the substrates in such encounters. The metallurgical connection between the surface layer and the splats is strengthened by the localized substrate melt. Because of the new metal-to-metal contact [44], the micro-hardness and binding strength of the coating are improved in this situation, and conduction with Alumina particles aided in the creation of the ideal surface roughness. The surface roughness facilitates the mechanical attachment of droplets to the substratum. Furthermore, current density has a significant impact because, as previously stated in the literature, it
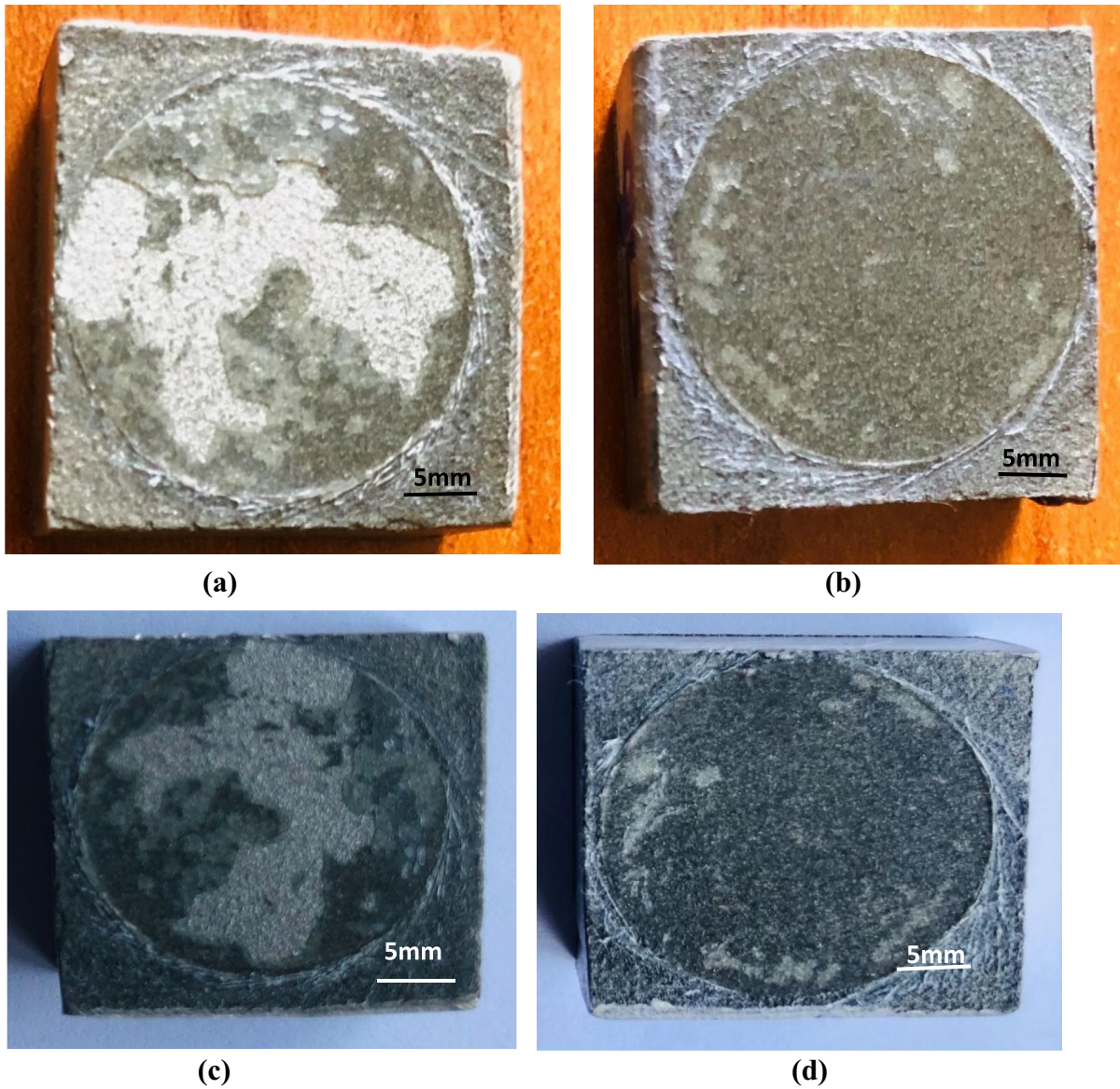
Fig. 6 Photographs of fractured surface Cr$_2$C$_3$ coatings at standoff distance (mm), powder feed rate (g/min) and current density (amps) of **a** 80, 50, 480 and **d** 80, 60, 480

improves bonding strength [45]. One of the key factors contributing to the high adhesive design strength may be that the spray operation in this case was carried out at the maximum current density of 480 amps.

Discussion

In the plasma spraying process, standoff distance plays a crucial role as it influences the performance, adhesion, and quality of the coating. In this study, the standoff distance was systematically varied during the coating of Al6061 alloy with Cr2C3 coatings, and its impact on coating qualities was assessed. Significant effects on coating thickness and porosity were observed in relation to the standoff distance. As the standoff distance increased, the coating thickness decreased, and porosity increased. This is attributed to the reduced efficiency of heat and energy transfer over longer distances. Closer standoff distances exhibited stronger substrate adherence, but also posed a risk of more frequent spalling due to overheating. The ideal standoff distance varies depending on the specific application needs. A shorter standoff distance may be preferable for applications prioritizing density and adhesion, while a longer standoff distance can be employed for applications requiring a thicker, more porous coating. Achieving

the desired coating performance necessitates a balance of these parameters.

Another influential factor affecting the quality and characteristics of plasma-sprayed coatings is the powder feed rate. The impacts of varying the powder feed rate during the deposition of Cr2C3 coatings on Al6061 alloy were examined. Results indicated a direct influence of the powder feed rate on the microstructure and hardness of the coating. Higher feed rates resulted in increased hardness due to improved coating density. However, very high feed rates led to a coarse microstructure and more splat boundaries, potentially compromising adherence. The choice of powder feed rate should align with desired coating qualities. A larger feed rate can be utilized to produce stronger coatings with enhanced wear resistance, provided it is carefully managed to prevent excessive porosity. Conversely, a lower feed rate may yield smoother coatings with less porosity, albeit at the expense of reduced hardness. Balancing these aspects is essential to meet the unique requirements of the application.

Current density, governing the energy input in the plasma spraying process and impacting coating adherence, microstructure, and overall quality, emerges as a crucial parameter. This study aimed to identify the optimal current density for coating Al6061 alloy with Cr2C3. Results revealed significant effects of changing the current density on coating adherence and microstructure. Higher current densities produced finer microstructures and improved adhesion. However, excessively high current densities could lead to excessive powder particle melting, resulting in increased porosity and diminished coating quality. Selection of current density should align with the intended coating properties. Higher current densities enable the production of dense coatings with enhanced mechanical characteristics, but precise management is essential to avoid overheating and preserve coating quality[46, 47].

Conclusion

The investigation into spraying process variables, including stand-off distance, powdered feed rate, and current density, was conducted using a Taguchi L_9 orthogonal array to achieve dense, compacted, and mechanically robust Cr_2C_3 coatings. The study yielded the following key findings:

1. Stand-off distance emerged as a crucial processing parameter for micro-hardness and permeability, while the powdered feed rate played a significant role in influencing strength properties, as indicated by the S/N ratio and analysis of variance (ANOVA) results.
2. Optimal values for achieving the lowest permeability were identified at a stand-off range of 60 rpm, powdered feed rate of 50 g/min, and current density of 480 amps.

Similarly, the highest micro-hardness was achieved at values of 60 rpm, 60 g/min, and 470 amps, while the best adhesion was attained at 60 rpm, 80 g/min, and 480 amps.
3. Minimal disparities were observed between projected and corrected R2 values for permeability and micro-hardness. Although bonding exhibited a greater variance than permeability or micro-hardness, the modified R2 value closely approached one, underscoring the appropriateness of the regression model.
4. Bond test results revealed broken surfaces, and scanning electron microscopy analysis of these surfaces unveiled mixed adhesion/cohesion type failures in Cr_2C_3 coatings.

Declarations

Conflict of interest The authors declare that they have no conflict of interest or personal relationships that could have appeared to influence the work reported in this paper.

References

1. C.-J.C.-X. Li, Q.-L. Zhang, S.-W. Yao, G.-J. Yang, C.-J.C.-X. Li, Plasma spraying of dense ceramic coating with fully bonded lamellae through materials design based on the critical bonding temperature concept. J. Therm. Spray Technol. **28**(1–2), 53–62 (2019)
2. J.-T. Gao, J.-H. Li, Y.-P. Wang, C.-J. Li, C.-X. Li, Performance and stability of plasma-sprayed 10×10 cm 2 self-sealing metal-supported solid oxide fuel cells. J. Therm. Spray Technol. **30**(4), 1059–1068 (2021)
3. H. Zhang, S. Liu, C. Li, C. Li, Deposition and oxidation behavior of atmospheric laminar plasma sprayed Mo coatings from 200 mm to 400 mm under 20 kW : numerical and experimental analyses, Surf. Coating. Technol. 400 (May) (2020)
4. S.-H. Liu, J.P. Trelles, A.B. Murphy, W.-T. He, J. Shi, S. Li, C.-J. Li, C.-X. Li, H.-B. Guo, Low-pressure plasma-induced physical vapor deposition of advanced thermal barrier coatings: microstructures, modelling and mechanisms. Mater. Today Phys. **21**, 100481 (2021)
5. D. Zhou, J. Malzbender, Y.J. Sohn, O. Guillon, R. Vaßen, Sintering behavior of columnar thermal barrier coatings deposited by axial suspension plasma spraying (SPS). J. Eur. Ceram. Soc. **39**(2e3), 482–490 (2019)
6. S.H. Liu, C.X.C.J. Li, H.Y. Zhang, S.L. Zhang, L. Li, P. Xu, G.J. Yang, C.X.C.J. Li, A novel structure of YSZ coatings by atmospheric laminar plasma spraying technology. Scripta Mater. Mater. **153**, 73–76 (2018)
7. S.-H. Liu, J.P. Trelles, C.-J. Li, H.B. Guo, C.-X. Li, Numerical analysis of the plasma-induced self-shadowing effect of

impinging particles and phases transformation in a novel long laminar plasma jet. J. Phys. Appl. Phys. **53**, 375202 (2020)

8. X. Wang, D. Fan, J. Huang, Y. Huang, Numerical simulation of arc plasma and weld pool in double electrodes tungsten inert gas welding. Int. J. Heat Mass Tran. **85**, 924–934 (2015)

9. E. Pfender, J. Fincke, R. Spores, Entrainment of cold gas into thermal plasma jets. Plasma Chem. Plasma Process. **11**(4), 529–543 (1991)

10. X. Chen, W. Pan, X. Meng, K. Cheng, D. Xu, C. Wu, What do we know about long laminar plasma jets. Pure Appl. Chem. **78**(6), 1253–1264 (2006)

11. Y. Tian, H. Zhang, X. Chen, A. MacDonald, S. Wu, T. Xiao, H. Li, Effect of cavitation on corrosion behavior of PLASMA-sprayed WC-10Co4Cr coating with post-sealing in artificial seawater. Surf. Coat. Technol. **397**, 126012 (2020)

12. N.C. Reddy, B.S.A. Kumar, M.R. Ramesh, P.G. Koppad, Microstructure and adhesion strength of Ni3Ti coating prepared by mechanical alloying and PLASMA. Phys. Met. Metall. **119**, 462–468 (2018)

13. M. Lobel, T. Lindner, T. Lampke, High-temperature wear behaviour of AlCoCrFeNiTi0.5 coatings produced by PLASMA. Surf. Coat. Technol. **403**, 126379 (2020)

14. N. Nagabhushana, S. Rajanna, M. Mathapati, M.R. Ramesh, P.G. Koppad, N.C. Reddy, Microstructure and tribological characteristics of APS sprayed NiCrBSi/flyash cenosphere/Cr2O3 and NiCrBSi/flyash cenosphere/Mo composite coatings at elevated temperatures. Mater. Res. Express **6**, 086451 (2019)

15. A. Milanti, V. Matikainen, G. Bolelli, H. Koivuluoto, L. Lusvarghi, P. Vuoristo, Microstructure and sliding wear behavior of Fe-based coatings manufactured with PLASMA and HVAF thermal spray processes. J. Therm. Spray Technol. **25**, 1040–1055 (2016)

16. K. Shivalingaiah, K.S. Sridhar, D. Sethuram, K.V.S. Murthy, P.G. Koppad, C.S. Ramesh, PLASMA sprayed Inconel 718/cubic boron nitride composite coatings: microstructure, microhardness and slurry erosive behavior. Mater. Res. Express **6**, 126i58 (2019)

17. G. Bolelli, L. Lusvarghi, T. Manfredini, F. Pighetti Mantini, R. Polini, E. Turunen, T. Varis, S.-P. Hannula, Comparison between plasma- and PLASMA-sprayed ceramic coatings. Part I Microstruct. Mech. Prop. Int. J. Surf. Sci. Eng. **1**, 38–61 (2007)

18. H. Singh, M.S. Grewal, H.S. Sekhon, R.G. Rao, Sliding wear performance of highvelocityoxy-fuel spray Al2O3/TiO2 and Cr2O3 coatings. Proc. Instit. Mech. Eng. Part J J. Eng. Tribol. **222**, 601–610 (2008)

19. X. Pang, K. Gao, A.A. Volinsky, Microstructure and mechanical properties of chromium oxide coatings. J. Mater. Res. **22**, 3531–3537 (2007)

20. S. Dong, B. Song, B. Hansz, H. Liao, C. Coddet, Microstructure and properties of Cr2O3 coating deposited by plasma spraying and dry-ice blasting. Surf. Coat. Technol. **225**, 58–65 (2013)

21. J.E. Fernandez, Y. Wang, R. Tucho, M.A. Martin-Luengo, R. Gancedo, A. Rincon, Friction and wear behaviour of plasma-sprayed Cr2O3 coatings against steel in a wide range of sliding velocities and normal loads. Tribol. Int.. Int. **29**, 333–343 (1996)

22. P. Zamani, Z. Valefi, Microstructure, phase composition and mechanical properties of plasma sprayed Al2O3, Cr2O3 and Cr2O3-Al2O3 composite coatings. Surf. Coat. Technol. **316**, 138–145 (2017)

23. S. Conze, M. Grimm, L.-M. Berger, S. Thiele, R. Drehmann, T. Lampke, Influence of simultaneous Cr2O3 and TiO2 additions on the microstructure and properties of APS alumina coatings. Surf. Coat. Technol. **405**, 126702 (2021)

24. N.C. Reddy, B.S.A. Kumar, H.N. Reddappa, M.R. Ramesh, P.G. Koppad, S. Kord, PLASMA sprayed Ni3Ti and Ni3Ti+(Cr3C2+20NiCr) coatings: Microstructure, microhardness and oxidation behaviour. J. Alloy. Compd. **736**, 236–245 (2018)

25. P. Fauchais, G. Montavon, G. Bertrand, Thermal spray fundamentals: from powder to part. Springer (2014)

26. L. Pawlowski, *The science and engineering of thermal spray coatings* (Wiley, 2008)

27. K. Goyal, Experimental investigations of mechanical properties and slurry erosion behaviour of high velocity oxy-fuel and plasma sprayed Cr2O3-50%Al2O3 coatings on CA6NM turbine steel under hydro accelerated conditions. Tribol. Mater. Surf. Interfaces. Mater. Surf. Interfaces **12**, 97–106 (2018)

28. N.C. Reddy, P.G. Koppad, H.N. Reddappa, M.R. Ramesh, E.R. Babu, T. Varol, Hot corrosion behaviour of PLASMA sprayed Ni3Ti and Ni3Ti+(Cr3C2+20NiCr) coatings in presence of Na2SO4-40%V2O5 at 650°C. Surf. Topogr. Metrol. Prop.Topogr. Metrol. Prop. **7**, 025019 (2019)

29. K. Goyal, H. Singh, R. Bhati, Behaviour of carbon nanotubes-Cr2O3 thermal barrier coatings in actual boiler. Surf. Eng. **36**, 124–134 (2020)

30. J.Y. Cho, S.H. Zhang, T.Y. Cho, J.H. Yoon, Y.K. Joo, S.K. Hur, The processing optimization and property evaluations of PLASMA Co-base alloy T800 coating. J. Mater. Sci. **44**, 6348–6355 (2009)

31. W. Tillmann, E. Vogli, I. Baumann, G. Kopp, C. Weihs, Desirability-based multicriteria optimization of PLASMA spray experiments to manufacture fine structured wearresistant 75Cr3C2-25(NiCr20) coatings. J. Therm. Spray Technol. **19**, 392–408 (2010)

32. J. Kawakita, S. Kuroda, T. Kodama, Evaluation of through-porosity of PLASMA sprayed coating. Surf. Coat. Technol. **166**, 17–23 (2003)

33. N. Puneeth, J. Satheesh, V. Koti, P.G. Koppad, M.R. Akbarpour, G.J. Naveen, Application of Taguchi's method to study the effect of processing parameters of Al6082/B4C/Al2SiO5 hybrid composites on mechanical properties. Mater. Res. Express **6**, 1065a1 (2019)

34. S. Ozel, E. Vural, M. Binici, Optimization of the effect of thermal barrier coating (TBC) on diesel engine performance by Taguchi method. Fuel **263**, 116537 (2020)

35. Y. Qin, Y. Wu, J. Zhang, S. Hong, W. Guo, L. Chen, H. Liu, Optimization of the HOVF spray parameters by Taguchi method for high corrosion-resistant Fe-based coatings. J. Mater. Eng. Perform. **24**, 2637–2644 (2015)

36. J.A. Gan, C.C. Berndt, Effects of standoff distance on porosity, phase distribution and mechanical properties of plasma sprayed Nd-Fe-B coatings. Surf. Coat. Technol. **216**, 127–138 (2013)

37. W. Tillmann, I. Baumann, P. Hollingsworth, I.-A. Laemmerhirt, Influence of the spray angle on the properties of PLASMA sprayed WC–Co coatings using (-10 + 2 μm) fine powders. J. Therm. Spray Technol. **272**, 272–279 (2013)

38. M. Bussmann, S. Chandra, and J. Mostaghimi, Numerical results of off-angle thermal spray particle impact, Thermal Spray 1999: United Thermal Spray Conference, E. Lugscheider, P.A. Kammer, Ed., Materials Park, Ohio and Dusseldorf, Germany, ASM International and DVS, 1999, p. 783-786

39. S. Vignesh, K. Shanmugam, V. Balasubramanian, K. Sridhar, Identifying the optimal PLASMA spray parameters to attain minimum porosity and maximum hardness in iron based amorphous metallic coatings. Defence Technol. **13**, 101–110 (2017)

40. A.S. Praveen, J. Sarangan, S. Suresh, B.H. Channabasappa, Optimization and erosion wear response of NiCrSiB/WC-Co PLASMA coating using Taguchi method. Ceram. Int. **42**, 1094–1104 (2016)

41. C.S. Ramachandran, V. Balasubramanian, P.V. Ananthapadmanabhan, Multiobjective optimization of atmospheric plasma spray process parameters to deposit yttria-stabilized zirconia coatings using response surface methodology. J. Therm. Spray Technol. **20**, 590–607 (2011)

42. R. Rajesh, S. Sumathi, Certain performance investigation on hybrid TiO2/Al2O3/MoS2 nanofiller coated 3Ø induction motor: a Taguchi and RSM based approach. Energy Rep. **6**, 1638–1647 (2020)

43. S. Brossard, P.R. Munroe, A.T.T. Tran, M.M. Hyland, Effects of substrate roughness on splat formation for Ni-Cr particles plasma sprayed onto aluminum substrates. J. Therm. Spray Technol. **19**, 1131–1141 (2010)

44. J. Matejicek, M. Vilemova, R. Musalek, P. Sachr, J. Hornik, The influence of interface characteristics on the adhesion/cohesion of plasma sprayed tungsten coatings. Coatings **3**, 108–125 (2013)

45. N. Pulido-Gonzalez, S. Garcia-Rodriguez, M. Campo, J. Rams, B. Torres, Application of DOE and ANOVA in optimization of PLASMA spraying parameters in the development of new Ti coatings. J. Therm. Spray Technol. **29**, 384–399 (2020)

46. T. Zhang, G. Mariaux, A. Vardelle, C.-J. Li, Numerical simulation of plasma jet characteristics under very low-pressure plasma spray conditions. Coatings **11**(6), 726 (2021). https://doi.org/10.3390/coatings11060726

47. S. Wang, S. Chen, M. Liu, Q. Huang, Z. Liu, X. Li, S. Xu, The effect of plasma spray parameters on the quality of Al-Ni coatings. Coatings **13**(12), 2063 (2023). https://doi.org/10.3390/coatings13122063